Quantum-Inspired Power System Reliability Assessment

Nima Nikmehr, *Senior Member, IEEE* and Peng Zhang, *Senior Member, IEEE*

***Abstract*—To enable an in-depth study of power system operation and planning, the assessment of standard reliability indices is inevitable. The Monte Carlo Simulation (MCS) approach is a broadly used method in replacing the analytical methods in reliability indices assessment. The accuracy of MCS, however, highly depends on the sampling size, and hence, a complicated system with large number of components requires a large sampling size and daunting computational effort. To address this shortcoming, this paper attempts to take advantage of potentials of the quantum computing (QC) for power system reliability assessment by realizing the following contributions: 1) an innovative quantum model designed for reliability assessment; 2) a quantum circuit that achieves the quadratic speed up compared to the classical MCS method; 3) an efficient quantum amplitude estimation (QAE) algorithm to accurately evaluate the reliability indices. The accuracy and efficacy of the quantum reliability method are extensively verified and demonstrated on both radial and mesh distribution systems.**

***Index Terms*—Quantum computing, Quantum amplitude estimation, Reliability assessment, Distribution systems**

I. Introduction

Assurance of continuity and quality of an electric power system in supplying the electrical demand can be precisely assessed by power system reliability analysis. The reliance of today's modern societies on reliable power sources has made the reliability analysis an indispensable and important study of power system planning and operation [1]. Nevertheless, power system reliability analysis remains to be a major challenge due to several aspects such as deep integration of distributed energy resources (DERs) and the resulting ubiquitous uncertainties, large number of power system components with heterogeneous failure and success models, ever growing smart and connected communities, and correlations and interdependence between grid components and DERs.

Classical Reliability Assessment. To assess the power system reliability, two main groups of methods, namely simulation-based methods and analytical methods are utilized. The analytical methods based on graph theory and the probability theory are generally applicable to small-scale systems [2]. With deep penetration of DERs and microgrids, the system states scale exponentially, which will result in complex computations and NP-hard solution difficulties [3], [4]. In [5], an analytical approach based on topology-depend method is utilized to derive the linear algebraic equations and then, assess the reliability indices of a distribution system. An interval reliability assessment method is introduced in [6] to formally enclose all reliability results under uncertainties, i.e., providing the estimates on upper and lower bounds of reliability and economic indices. In [7], the authors have developed a Bayesian method to analyze the reliability of DC microgrids considering the linearized power flow formulation. Moreover, the developed method assesses the impact of renewable energies in improving the reliability of microgrids through quantifying new reliability indices. An analytical method based on continuous time Markov chain merges all high order contingencies into a single state, and evaluates the reliability indices in composite generation and transmission systems [8]. Additionally, the simulation-based methods such as Monte Carlo Simulation (MCS) technique requires many samples and computational effort to obtain the probability distribution function of a reliability index [9, p.400]. One category of the MCS methods is the sequential MCS (SMCS) where the chronology of failures of power system components, and variations associated with DERs and loads are modeled [10]. Although SMCS is useful to assess the frequency-based reliability indices, to obtain accurate results, the computational expense is higher [11]. Additionally, the usage of time-series methods such as the auto regressive moving average model in SMCS requires hourly data from the system parameters, which are generally unavailable [12]. To mitigate the dependence of the random parameters to the detailed chronological nature, non-sequential MCS (NMCS) method is taken into account, where probability distribution functions can be utilized for the system variables [13], [14]. However, this method is not a suitable alternative for sequential MCS method to assess the frequency-based reliability indices [15]. The pseudo-MCS [16] and quasi-MCS [17] are other variants of MCS method that can achieve speed-up advantage over SMCS. However, these methods suffers the incomplete system chronology, and thereby non-cumulative frequency of a system. An alternative approach to calculate a system reliability is to use a reliability-constrained optimization model [18], which is generally formulated as a mixed-integer linear programming (MILP) problem. However, the optimization-based approaches suffer the intractability of finding the global optimality. In [19], a linear-programming-based model is presented to assess the reliability indices in distribution systems, and the network topology is determined after solving the optimal power flow problem. A reliability-constrained optimization model based on load restoration through tie-lines is studied in [20]. In [21], to assess and improve the reliability of a distribution system, the developed optimization-based model considers the optimal placement of circuit breakers and switches. The machine learning techniques have introduced a new application in power system reliability assessment. In [22], a classification algorithm is used to classify the system sates by requiring the optimal power flow in training stage. However, most classification algorithms are unable to assess the energy and frequency indices of com-

This work was supported in part by the Advanced Grid Modeling Program under Department of Energy's Office of Electricity under Agreement No. 37533, and in part by the National Science Foundation under Grant Nos. OIA-2040599 and OIA-2134840. This work relates to Department of Navy award N00014-20-1-2858 issued by the Office of Naval Research. The United States Government has a royalty-free license throughout the world in all copyrightable material contained herein. *(Corresponding author: Peng Zhang.)*

N. Nikmehr and P. Zhang are with the Department of Electrical and Computer Engineering, Stony Brook University, Stony Brook, NY 11794, USA (e-mail: nima.nikmehr@stonybrook.edu; p.zhang@stonybrook.edu).

posite systems [23]. In [24], the reliability indices of integrated energy systems are calculated using a machine learning method combining Random Forest method and XGBoost regression algorithm, and SMCS is employed to generate the required data. In [25], a SMCS incorporating dynamic Bayesian belief networks for generating the probability distributions of solar and wind energies and a rolling-horizon unit commitment as an optimization model is developed for evaluating distribution reliability indices. Although some existing machine learning methods can improve the computational time in evaluating the reliability indices, they need to be carefully trained to achieve accurate results. In this paper, to resolve the aforementioned problems, a promising technology based on quantum computing (QC) is devised for power system reliability assessment. The potential of QC has been already proved in solving combinatorially complex unit commitment problem where a fast convergence is reached compared to the classical optimization methods [26].

General Discussion on Quantum Computing. To perform QC for information processing purposes, the laws of quantum physics are used in superconducting devices. A future noise-free quantum computer has the potential to achieve quantum supremacy in solving large-scale problems by running quantum speed-up solutions that cannot be simulated in classical counterparts [27]. The core idea of utilizing the QC algorithm in estimating the expected value of an uncertain variable is to reduce the number of uses of a randomized algorithm in classical MCS technique [28]. A correct design of a quantum algorithm containing various gates and unitary operators can end up in an acceptable approximation with quadratic speed-up. Compared to the classical MCS technique where the convergence rate is $O(\frac{1}{\sqrt{S}})$ with total samples S [29], the authors in [30]–[32] have shown that the quadratic speed up with convergence $O(\frac{1}{S})$ can be achieved by quantum algorithms.

Quantum Computing Applications. An early report [33] suggested potential applications of quantum computing in power systems without providing executable quantum models. The application of quantum computing on a decoupled AC power flow is shown in [34] where the quantum-inspired fast decoupled power flow is first developed and then, Harrow-Hassidim-Lloyd (HHL) quantum algorithm is introduced as an applicable quantum algorithm. Later, a quantum electromagnetic transients program (QEMTP) based on a modified Harrow-Hassidim-Lloyd (HHL) algorithm is devised [35]. Based on this success, a shallow-depth, logarithmical-width variational quantum circuit (VQC) is developed, which allows for QEMTP simulations on today's noisy-intermediate-scale quantum (NISQ) computers [36]. A quantum shifted frequency analysis (QSFA) for accelerating QEMTP has also been developeds [36]. In [37], the quantum-inspired version of particle swarm optimization (QPSO) is developed where instead of classical mechanics, the quantum mechanics is employed to show the quantum state of particles using wave function. Although the quantum version of PSO has a better convergence performance compared to the original version of the PSO, in lights of less control parameters, the obtained solution might be local optima. The accelerated version of QPSO is used in [38] to maximize the reliability of the system where an optimization-based model is employed. However, since the current optimization problems should be in a quadratic unconstrained binary optimization (QUBO) framework, the proposed optimization model is not applicable to quantum machines. In [26], the applicable quantum optimization models, which can be dealt with the quantum machines are discussed for the distributed unit commitment problem. To decrease the delays of network function visualization technology, an integer linear programming model is developed in the form of QUBO to be solved using quantum annealing machine [39]. However, the utilized optimization solver is unable to assign continuous variables to the system variables and parameters. Among the quantum algorithms, Quantum Amplitude Estimation (QAE) algorithm [31], which takes advantage of the idea of Grover's search algorithm [40], has already proved the quadratic speedup and convergence over the classical MCS technique in estimating an uncertain variable. Currently, a main application of QAE is in the finance field in which the uncertain nature of finance parameters necessitates the stochastic analysis. In [41], the value at risk and conditional value at risk measures are calculated using QAE with a quadratic convergence rate. In [42], financial derivative pricing is solved using a hybrid quantum-classical algorithm in which quantum Generative Adversarial Networks is taken into account to model the probability distributions, and then QAE solves derivative pricing problem. The advantageous performance of QAE over MCS technique can be found in the implementation of different models of option pricing using the maximum likelihood estimation method [43] instead of using quantum phase estimation [44, P.221].

Contributions. To address the gap in the literature review on drawbacks of classical MCS and analytical methods, this paper unlocks the potential of quantum computing in power system reliability evaluation. To take advantage of the quantum computational framework, this paper firstly contributes to developing a quantum-supported power system reliability model such that the required reliability indices are assessed. Then, a QAE-enabled reliability algorithm is established to calculate the power system reliability indices where the convergence speed-up is achieved compared to the classical MCS.

Organization. In Section II, a quantum computing background is firstly explained and then, the general steps to integrate the classical MCS into the quantum circuit is presented. In Section III, the quantum circuit of QAE algorithm is explained and shown on preparing the practical circuit to execute the QAE algorithm in a real quantum computer. In Section IV, the quantum-amenable model of power system reliability indices is formulated. In Section V, the results of reliability indices obtained by QC are compared to those from classical methods.

II. Quantum Computing Background

In this section, firstly, a general preview of quantum computing is given. Then, the required quantum-amenable steps to execute the MCS in a quantum circuit are listed.

A. Basics of quantum computing

The laws of quantum mechanics enable the Quantum computers to solve the problems using new quantum-oriented algorithms. In one of the prevalent types of quantum computers, the quantum circuit model is utilized, in which quantum bits (qubits) are the basic units of quantum information [45]. Thanks

to the superposition feature [46], quantum computers can be in multiple states, which means that unlike the digital computers including b bits, quantum computers can hold 2^b bits of information before measured in basis states $|0\rangle$ and $|1\rangle$. Therefore, in a system with a single qubit, the superposition principle of qubit ψ indicates a linear combination of possible configurations as $|\psi\rangle = \alpha|0\rangle + \beta|1\rangle$, where $|\alpha|^2$ and $|\beta|^2$ describe the probabilities for the system to be in either states $|0\rangle$ or $|1\rangle$, respectively. According to the Born rule, the measurement of a qubit should yield $|\alpha|^2 + |\beta|^2 = 1$ [44, P.15]. Therefore, in a generic form, the superposition of a qubit including b bit-string basis states can be defined as $|\psi\rangle^b = \sum_{x\in\{0,1\}^b} \psi(x) \cdot |x\rangle$. Additionally, a quantum register in quantum computers is used to define a system with multiple qubits, which is realized via the Hilbert space. In that system, the tensor products of available qubits can mathematically represent the quantum register as $|\psi\rangle = |\psi_1\rangle \otimes |\psi_2\rangle \otimes \cdots \otimes |\psi_N\rangle = |\psi_1\psi_2 \dots \psi_N\rangle$, where N is the total number of qubits.

To develop a complex quantum circuit, quantum gates are imperative components of quantum computers to manipulate the input state-vectors and generate an output. The quantum gates are reversible and mathematically defined by unitary matrices such that the quantum gate U can be represented as $U \cdot U^\dagger = I$, where $U^\dagger$ is conjugate transpose of a complex square matrix U. To solve a problem using a quantum algorithm, firstly a quantum gate which can be a single-qubit gate, a two-qubit gate or a multi-qubit gate, is applied to either a qubit or multiple qubits. Afterwards, the state of the qubit(s) is changed accordingly. Finally, there exists a measuring unit at the end of the circuit to measure one or more qubits [47]. In Fig. 1, a quantum schematic of a sample system is depicted.

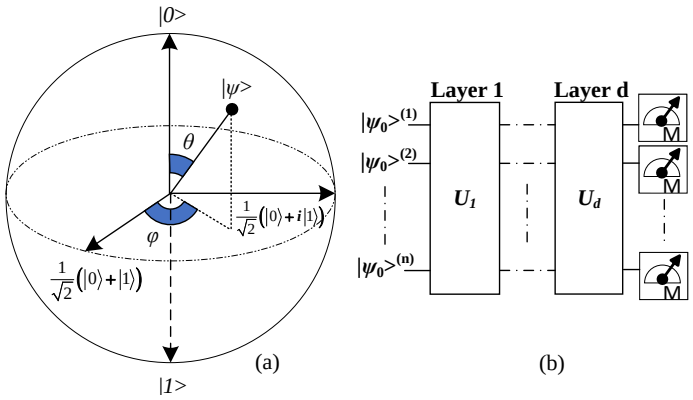

Fig. 1. (a) A visualization to a single-qubit sate which is described as $|\psi\rangle = cos(\frac{\theta}{2})|0\rangle + e^{i\phi}sin(\frac{\theta}{2})|1\rangle$, where angles θ and ϕ are used to map the state ψ to a point in Bloch sphere. (b) A schematic of a quantum circuit, where the initial n-qubit register state is manipulated after being applied to d layers of unitary operators, and finally, the quantum state $|\psi\rangle$ is measured, which results in dynamics of the original system.

B. Quantum-oriented steps for integrating the classical MCS

In solving a problem using the classical Monte Carlo method, three main steps should be taken into account: first, the uncertain parameters should be modeled as random variables to start the stochastic procedure. Therefore, we can model all the random variables as $X = \{X_1, X_2, \cdots, X_{\mathcal{R}}\}$, where $\mathcal{R}$ is the total number of random variables. In the second step, S samples should be generated for each random variable using the probability distribution function of each variable. Thus, each random variable with S samples can be described as $\{x_1, x_2, \cdots, x_S\}$, where x is a random sample of a variable. Finally, the expected value of a real-valued function $f(x)$ for each random variable is calculated as follows:

$$E[f(X_j)] = \sum_{i=1}^{S} \frac{1}{S} f(X_{i,j}),\ \forall j \in \{1, 2, \cdots, \mathcal{R}\}. \quad (1)$$

The estimated expected value using the iterative process of Monte Carlo method can be improved by increasing the number of sampling. According to the central limit theorem, the convergence of estimated expected value depends on the sampling size that is $O(\frac{1}{\sqrt{S}})$ [48, P.89].

Based on the aforementioned steps for the classical Monte Carlo simulations, a quantum circuit to solve a problem under uncertainties should include the following quantum blocks:

- The first block of the quantum circuit should generate a probability distribution function with a number of quantum samples.
- The second block of the quantum circuit should include a unitary operator to calculate the function of random variables.
- Finally, a quantum algorithm is utilized to measure the amplitude of a state so that an estimation of expected value of the function containing the uncertain variables is obtained.

III. Quantum Amplitude Estimation Algorithm

In this section, firstly, the execution steps of the QAE algorithm are explained by introducing the required quantum blocks. In the second subsection, a practical quantum circuit to implement the QAE algorithm is discussed.

A. QAE algorithm implementation

The QAE algorithm aims at estimating the function of uncertain parameters quadratically faster than the MCS method [49], [50]. The number of usage of the quantum algorithm in estimating a function of uncertain variables is quadratically decreased compared to the classical MCS [28], meaning as long as the classical randomize procedure is not involved in the QAE algorithm, the quantum speed-up is achievable.

A big picture of the QAE algorithm is shown in Fig. 2. There exist three main quantum blocks including $\mathcal{P}$, $\mathcal{H}$ and L. The quantum block $\mathcal{P}$ is employed to load the distribution function of a random variable. The quantum operator $\mathcal{H}$ is used to rotate the Bloch vector around the y axis by angle θ. To have a better estimation of a function, the quantum block L is used.

To implement the QAE algorithm, three main steps including the estimation procedure using QAE, loading the probability distribution functions of random variables, and calculating the function $f(x)$ of the random variable x should be considered.

1) Estimation procedure of QAE: In this subsection, the required quantum computational blocks of QAE are represented to estimate the expected value. Also, the performance of QAE in decreasing the number of measurements is discussed.

This article has been accepted for publication in IEEE Transactions on Power Systems. This is the author's version which has not been fully edited and content may change prior to final publication. Citation information: DOI 10.1109/TPWRS.2022.3204393

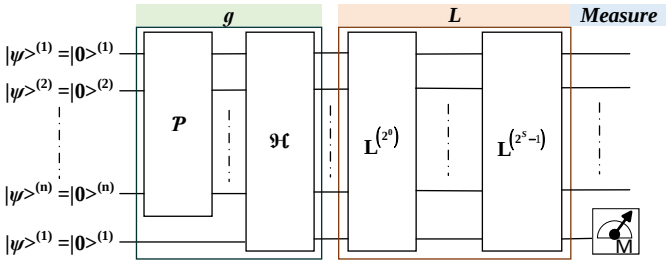

Fig. 2. Quantum circuit of MCS integration as an amplitude estimation

According to the quantum circuit in Fig. 2, several quantum blocks should be implemented in sequence. In the first block, an algorithm called $\mathcal{P}$ is considered on an n-qubit register $|0\rangle_n$. The algorithm outputs:

$$\mathcal{P}\,|0\rangle_n = \sum_{i=0}^{2^n-1} \sqrt{p(x_i)} \cdot |x_i\rangle_n \,. \tag{2}$$

where, the algorithm outputs the n-bit string result x with probability $p(x)$.

In the second block of the quantum circuit, the unitary operator $\mathcal{H}$ is applied to $(n+1)$ qubits. In this step, a rotation is executed onto an ancilla qubit. Therefore, in addition to n-qubit register $|x\rangle_n$ obtained using operator $\mathcal{P}$, there exists a qubit register $|0\rangle$. The operator $\mathcal{H}$ outputs:

$$\mathcal{H}\,|x\rangle_n\,|0\rangle = |x\rangle_n \left(\sqrt{f(x)} \cdot |1\rangle + \sqrt{1-f(x)} \cdot |0\rangle\right). \tag{3}$$

where, $f(x)$ is a function $f(x) : \{0,1\}^n \to \mathbb{R}$ which is mapped to real numbers from n-bit strings.

The output state ψ is resulted after applying quantum blocks $(\mathcal{P} \otimes I)$ and $\mathcal{H}$ to the states $|0\rangle_n\,|0\rangle$:

$$\begin{aligned} |\psi\rangle &= \mathcal{H}(\mathcal{P} \otimes I) \cdot |0\rangle_n\,|0\rangle \\ &= \sum_{i=0}^{2^n-1} \left[\sqrt{p(x_i)} \cdot |x_i\rangle_n \left(\sqrt{f(x_i)} \cdot |1\rangle + \sqrt{1-f(x_i)} \cdot |0\rangle\right)\right]. \end{aligned} \tag{4}$$

where, I is the identity operator.

To rewrite the obtained state (4) in a straightforward manner, we firstly define two orthonormal bases, in which $y = \sum_{i=0}^{2^n-1} p(x_i) \cdot f(x_i)$:

$$|\psi_0\rangle = \frac{\sum_{i=0}^{2^n-1} \sqrt{p(x_i)} \cdot \sqrt{1-f(x_i)} \cdot |x_i\rangle_n\,|0\rangle}{\sqrt{1-y}}, \tag{5a}$$

$$|\psi_1\rangle = \frac{\sum_{i=0}^{2^n-1} \sqrt{p(x_i)} \cdot \sqrt{f(x_i)} \cdot |x_i\rangle_n\,|1\rangle}{\sqrt{y}}. \tag{5b}$$

where, $|\psi_0\rangle$ and $|\psi_1\rangle$ are normalized states with n qubits.

Using (5a) and (5b), the state ψ as the output state passing through the unitary operator g, is described as follows:

$$|\psi\rangle = \sqrt{1-y} \cdot |\psi_0\rangle + \sqrt{y} \cdot |\psi_1\rangle \,. \tag{6}$$

where, the purpose of QAE is to estimate the probability of measurement $|1\rangle$, which is equal to $(\sqrt{y})^2 = \mathbb{E}[f(x)]$ [31]. Suzuki, et al [43] improved the estimation of expected value of an unknown parameter by amplifying the probability of measurement $|1\rangle$. In general, the prepared state $|\psi\rangle_{n+1}$ is described as follows in terms of $\theta \in \left[0, \frac{\pi}{2}\right]$ to realize $sin^2\theta = f(x)$:

$$g\,|0\rangle_{n+1} = cos(\theta) \cdot |\psi_0\rangle_n\,|0\rangle + sin(\theta) \cdot |\psi_1\rangle_n\,|1\rangle \,. \tag{7}$$

According to Fig. 2, there exists a block L with s sampling qubits and $S = 2^s$ application of operator L. The operator $L = g \cdot K_0 \cdot g^\dagger \cdot K_{\psi_0}$ with $K_0 = 1 - 2\,|0\rangle\langle 0|$ and $K_{\psi_0} = 1 - 2\,|\psi_0\rangle\,|0\rangle\langle\psi_0|\langle 0|$ is employed in the quantum circuit to obtain the efficient estimation of y.

To amplify the probability of measured state $|1\rangle$, the unitary operator L is applied on the prepared state by (7) for s times, which yields:

$$\begin{aligned} L^s\,|\psi\rangle_{n+1} = &\, cos(\theta(2s+1)) \cdot |\psi_0\rangle_n\,|0\rangle \\ &+ sin(\theta(2s+1)) \cdot |\psi_1\rangle_n\,|1\rangle \,. \end{aligned} \tag{8}$$

where, similar to (8), the unknown parameter $f(x)$ is estimated as $sin^2(\theta(2s+1))$ after applying the operator L.

In Fig. 3, the full circuit of QAE is illustrated.

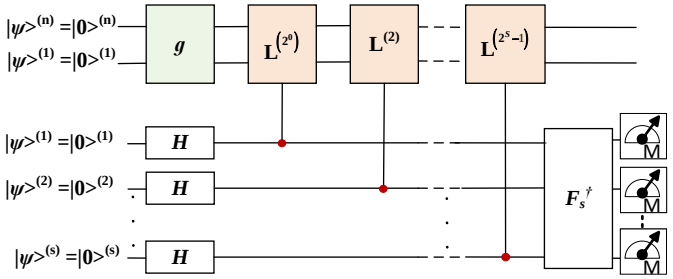

Fig. 3. Quantum circuit of QAE. Blocks H and $F_s^\dagger$ represent the Hadamard gate and the inverse Quantum Fourier Transform, respectively.

According to Fig. 3, Hadamard gates (H) are utilized to initialize the qubits to superposition states. Afterwards, the qubits in superposition states control S applications of operator L. The ancilla qubits are finally measured after performing an inverse Quantum Fourier Transform, which gathers the amplitudes of states [31]. The measurement results in integer values $z \in \{0, 1, \cdots, S-1\}$, which is mapped to the estimator for y as follows:

$$\hat{y} = sin^2\left(\frac{z \cdot \pi}{S}\right). \tag{9}$$

where, $\hat{y}$ is estimated in S calls to the oracle with the following error with a probability of at least $\frac{8}{\pi^2}$ [31], [51]:

$$|y - \hat{y}| \leq \frac{2\pi\sqrt{y(y-1)}}{S} + \frac{\pi^2}{S^2} = \mathcal{O}\left(\frac{1}{S}\right). \tag{10}$$

which shows a quadratic speed-up compared to the classical MCS method with the convergence rate of $\mathcal{O}\left(\frac{1}{\sqrt{S}}\right)$ [52]. This result shows that integrating the classical MCS method in the quantum circuit achieves the same estimation accuracy, but with quadratically less samples [28].

The circuit depth is the longest path from the input to the output of the circuit. The number of time steps determines the depth of the circuit. Additionally, the number of gates in the longest circuit path is proportional to the depth of the circuit, which is an integer number. To reduce the circuit depth of the QAE algorithm, Suzuki *et al.* [43] have eliminated the

quantum phase estimation with the guaranteed quadratic speed-up. Another advantage is that the dependency of the QAE algorithm to qubits is reduced. In this model, to estimate θ in (8), a maximum likelihood estimation methods with S number of operator L and $\mathcal{W}$ shots for each experiment is used, which yields the estimation error as $\mathcal{O}\left(\frac{1}{S\cdot\sqrt{\mathcal{W}}}\right)$, still resulting in a quadratic speed-up.

2) Quantum block for probability distribution function: To load the probability distribution function corresponding to the random variable, the quantum register takes the random variable and assigns a possible value with the corresponding amplitude as its probability using the basis state. As shown in Fig. 2, the operator $\mathcal{P}$ takes an n-qubit state $|\psi\rangle$ and yields (2) with a random variable x with its probability $p(x)$. Therefore, to estimate the values of a random variable x using n qubits, the QAE algorithm maps the variable to the integer interval $\{0,1,\cdots,2^n-1\}$. Then, the random variable is described in a quantum state as (2) such that $\sum_{i=0}^{2^n-1} p_i(x)=1$.

3) Quantum block for calculating the function f(x) of the random variable x: According to operator g, the expected value of $f(x)$ is the amplitude of state $|\psi_1\rangle$ described in (4)-(6). In this subsection, we explain how to create the quantum circuit for operator g such that the expected value of function f of the variable x is achieved. To do this, the generated operator should execute the following mapping:

$$\begin{aligned}\sum_{i=0}^{2^n-1}\sqrt{p_i}\cdot|i\rangle_n|0\rangle \rightarrow \sum_{i=0}^{2^n-1}\sqrt{p_i}\cdot|i\rangle_n\cdot\\ \left[cos\left(c\cdot\hat{f}_i+\frac{\pi}{4}\right)|0\rangle+sin\left(c\cdot\hat{f}_i+\frac{\pi}{4}\right)|1\rangle\right].\end{aligned} \tag{11}$$

where, the function f is mapped to the integer values $i\in\{0,1,\cdots,2^n-1\}$. Also, $\hat{f}$ is defined as a scaled version of function f, which is defined as following:

$$\hat{f}_i=2\frac{f_i-f_i^{min}}{f_i^{max}-f_i^{min}}-1. \tag{12}$$

where, f_i^{min} and f_i^{max} are the minimum and maximum values of function $f(x)$.

The parameter c is chosen in the range $[0,1]$. As mentioned in the previous subsection, the probability of ancilla qubit in state $|1\rangle$ leads toward the estimation of expected value of function f in the form of $\sum_i p(i)\cdot sin^2\left(c\cdot\hat{f}+\frac{\pi}{4}\right)$. Using the fact that $sin^2\left(\hat{x}+\frac{\pi}{4}\right)\approx\hat{x}+\frac{1}{2}$ for small $\hat{x}$, the following approximation for the probability of state $|1\rangle$ is obtained [41]:

$$sin^2\left(c\cdot\hat{f}_i+\frac{\pi}{4}\right)=c\cdot\hat{f}_i+\frac{1}{2}+\mathcal{O}\left(c^3\cdot\hat{f}_i^3\right). \tag{13}$$

The first order approximation in (13) yields the convergence rate of $\mathcal{O}\left(\frac{1}{S^{\frac{2}{3}}}\right)$ which is still faster than the classical MCS method [41]. To improve the convergence rate of QAE, higher order approximation and implementation of the quantum circuit is required to achieve the convergence rate of $\mathcal{O}\left(\frac{1}{S}\right)$.

B. Practical quantum circuit of QAE algorithm

In subsection III-A, the quantum circuit of QAE is explained in theoretic manner. To realize the quantum circuit for current quantum computers, this subsection provides practical quantum gates and blocks for the QAE algorithm.

Constructing the operator $\mathcal{P}$: The first unitary operator in the quantum circuit of the QAE algorithm is $\mathcal{P}$, which acts on n-qubit states (see Fig. 2). Constructing the operator $\mathcal{P}$ yields the quantum state described in (2), which represents the probability distribution of a random variable. Generally, it is shown that the complexity of $\mathcal{O}(2^n)$ is needed to consider the required number of quantum gates in constructing the operator $\mathcal{P}$ [53]. However, many distribution functions such as log-concave distribution have the polynomial complexity $\mathcal{O}(n)$ [54].

To model the probability distribution in the quantum circuit of the QAE algorithm, we can use different quantum gates in different designs.

In one of the quantum models, Hadamard gates are used to construct the operator $\mathcal{P}$ [43]. The Hadamard gate puts a qubit in a superposition state and is represented by the following matrix [44, P.19]:

$$H=\frac{1}{\sqrt{2}}\begin{bmatrix}1 & 1\\ 1 & -1\end{bmatrix}. \tag{14}$$

A generic form of applying Hadamard gate into an n-qubit state ($H^{\otimes n}$) is defined as follows, which is the output of the operator $\mathcal{P}$:

$$H^{\otimes n}|\psi\rangle_n=\frac{1}{\sqrt{2^n}}\sum_{i\in\{0,1\}^n}(-1)^{i\cdot\psi}|i\rangle_n. \tag{15}$$

According to (15), utilizing the Hadamard gate results in a probability distribution with an equal probability $\frac{1}{2^n}$ for all existing states. In the next quantum model to establish the probability distribution function, single-qubit Y-rotations are used. To do this, Pauli matrix Y, which is a 2 by 2 complex Hermitian and unitary matrix $\sigma_y=\begin{bmatrix}0 & -i\\ i & 0\end{bmatrix}$, is utilized to create the rotation operator $R_y(\theta)$ which rotates the Bloch vector (see Fig. 1(a)) by angle θ around the axis y. The Y-rotation operator is defined as follows:

$$\begin{aligned}R_y(\theta)=&e^{-i\frac{\theta}{2}Y}=cos\left(\frac{\theta}{2}\right)I-isin\left(\frac{\theta}{2}\right)Y\\ &=\begin{bmatrix}cos\left(\frac{\theta}{2}\right) & -sin\left(\frac{\theta}{2}\right)\\ sin\left(\frac{\theta}{2}\right) & cos\left(\frac{\theta}{2}\right)\end{bmatrix}.\end{aligned} \tag{16}$$

In Fig. 4, two different quantum circuits for operator $\mathcal{P}$ are depicted. Using different quantum gates results in different probability distribution functions. In Fig. 4, three qubits are used to prepare the distribution function of random variable x. In general, n number of qubits prepare 2^n samples or values for a random variable. Thus, in a 3-qubit quantum register, the random variable x takes eight different values. For each value, a quantum state from the set $|\psi\rangle=\{|000\rangle,|001\rangle,\cdots,|111\rangle\}$ is assigned. Moreover, in Fig. 4(b), there is a CNOT gate to generate the required quantum states for each value. The CNOT gate is applied to two qubits and flips the second qubit (target qubit) if and only if the first qubit (control qubit) is in state $|1\rangle$.

It is noted that different probability distribution functions are derivable based on the utilized quantum gates and the architecture of gates. In [55], the loaded log-normal distribution uses different numbers of Y-rotation and CNOT gates compared to the Fig. 4(b).

Constructing the operator g: As theoretically explained in subsection III-A and depicted in Fig. 2, the operator g consists

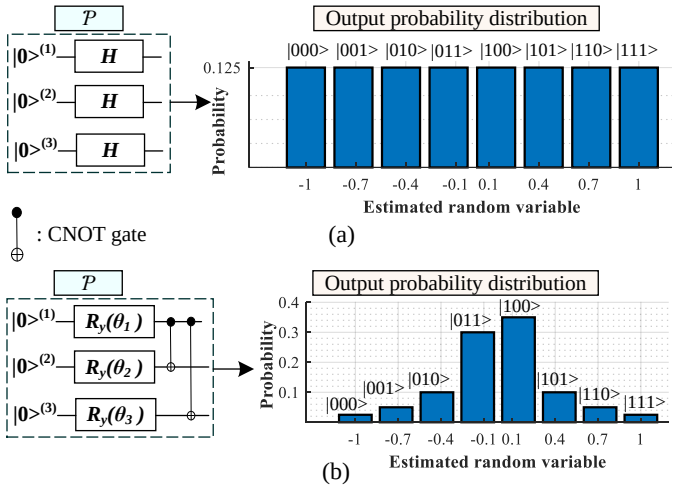

Fig. 4. Loading distribution function in the quantum circuit of QAE consisting of 3 qubits. (a) Applying Hadamard gate in operator $\mathcal{P}$ yields a distribution function with equal probability for each quantum state. (b) Applying Y-rotation with angle θ and controlled NOT gate (CNOT) result in a distribution function with different probabilities for quantum states.

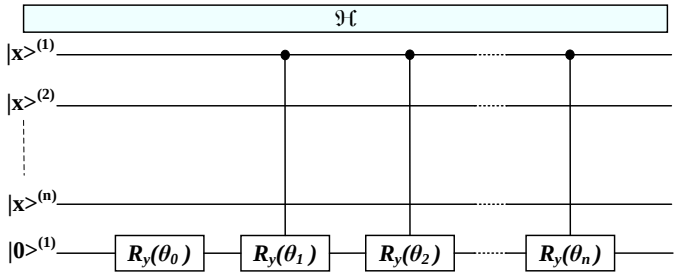

Fig. 5. Quantum circuit of operator $\mathcal{H}$ including n-qubit state $|x\rangle$ and Y-rotation with angle θ

of two quantum blocks $\mathcal{P}$ and $\mathcal{H}$. Here, we show how to map the aforementioned estimation of a function $f(x)$ in (3) to a practical quantum circuit using quantum gates.

To estimate $f(x)$, the operator g rotates an ancilla using controlled Y-rotations ($R_y(\theta)$). The operator g acts on an (n+1)-qubit state yielding (7), i.e.:

$$\begin{aligned} |x\rangle_n |0\rangle &\rightarrow |x\rangle_n R_y(\theta_x) |0\rangle \\ &\rightarrow |x\rangle_n (cos(\theta) \cdot |0\rangle + sin(\theta) \cdot |1\rangle) . \end{aligned} \tag{17}$$

In (17), an n-qubit state $|x\rangle$ is applied to $R_Y(\theta_n)$ with angle θ to create the block $\mathcal{H}$ as shown in Fig. 5.

Now, the quantum circuit of operator g, which is a combination of operators $\mathcal{P}$ and $\mathcal{H}$, is depicted for any probability distribution functions as Fig. 6.

Therefore, we can model the operator g by a Y-rotation with the following angle for y (probability of measurement $|1\rangle$):

$$\begin{aligned} g &= R_y(\theta_y), \\ \theta_y &= 2arcsin(\sqrt{y}) . \end{aligned} \tag{18}$$

Constructing the operator L:

In the QAE algorithm, we exploit the operator L with a total of S samples to achieve an efficient estimation of probability measurement $|1\rangle$. Therefore, instead of measuring state $|1\rangle$ after the operator g, L operator is involved between operator g and measuring units to amplify the probability of measurement $|1\rangle$.

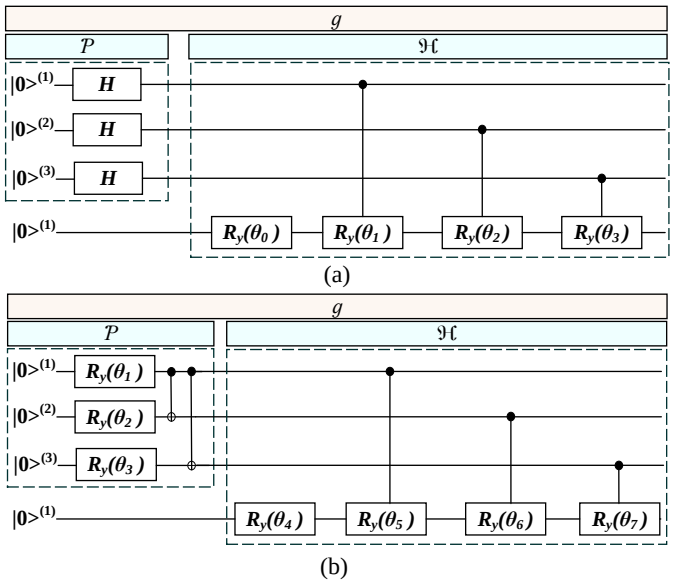

Fig. 6. Quantum circuit of operator g including 3-qubit input and an ancilla. (a) Operator g when a distribution function with equal probability for all quantum states is loaded. (b) Operator g when a distribution function with different probabilities for each quantum state is loaded.

It is proved that $S = 2^s$ applications of operator L in the form of $(L)^s g |0\rangle_{n+1}$ leads toward at least $4s^2$ measurement probability of $|1\rangle$ higher than applying $g |0\rangle_{n+1}$ [43]. In Fig. 7, the quantum circuit corresponding to operator $L = g \cdot K_0 \cdot g^\dagger \cdot K_{\psi_0}$ with a single application of L is drawn.

As seen in Fig. 7, there are several quantum gates in the quantum circuit. Hadamard gate is exploited to encode the distribution function. Y-rotation gate with angle θ is the core component of QAE algorithm in estimating the probability of measurement $|1\rangle$. Additionally, Pauli-X and Pauli-Z are used to rotate a vector around the x and z axes of the Bloch sphere, respectively, by π Radians. Pauli-X, which is defined as the matrix $X = \begin{bmatrix} 0 & 1 \\ 1 & 0 \end{bmatrix}$, is equivalent to NOT gate in classical computers. This matrix maps state $|0\rangle$ to state $|1\rangle$ and vice versa. Moreover, Pauli-Z is defined as the matrix $Z = \begin{bmatrix} 1 & 0 \\ 0 & -1 \end{bmatrix}$, and keeps state $|0\rangle$ unchanged while state $|1\rangle$ is mapped to $-|1\rangle$. In a quantum computer, the operator L is modeled as $(L)^s = R_y(2s\theta_y)$.

IV. Quantum Amplitude Estimation Algorithm for Power System Reliability

In this section, we aim at applying the QAE algorithm to power system reliability calculation. To this end, without loss of generality, we provide a brief recapitulation of classical distribution reliability assessment. Then, the quantum-amenable reliability evaluation is discussed using the QAE algorithm.

A. Distribution system reliability assessment from a classical viewpoint

A distribution system consists of various components such as distributions lines, cables, disconnects, busbars and switches. In the MCS method, first, the system states should be generated.

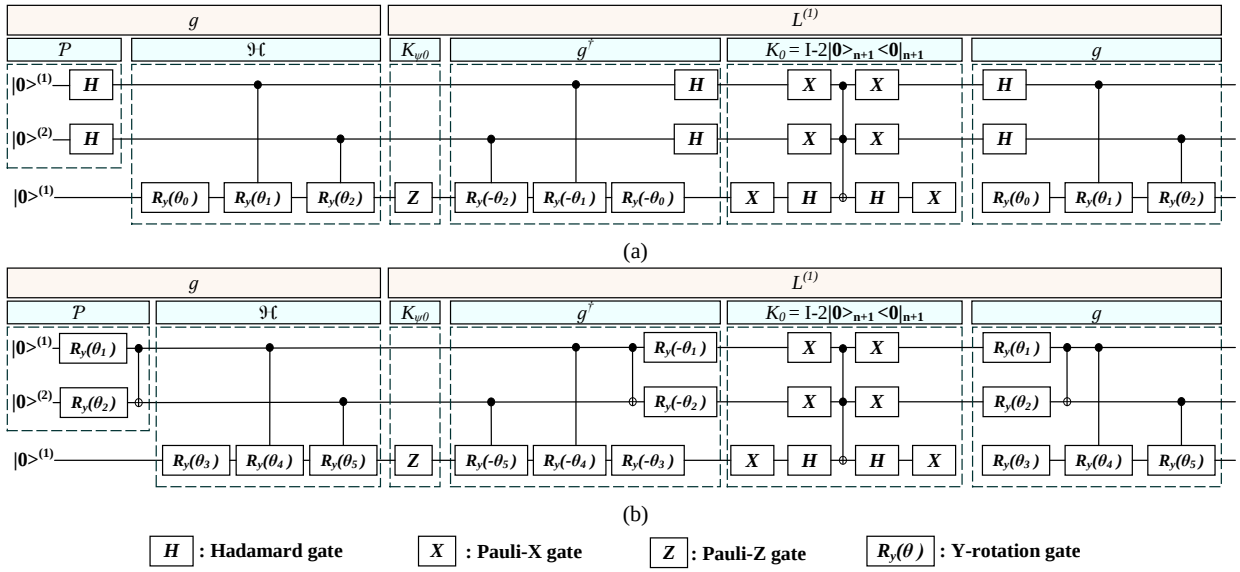

Fig. 7. A part of quantum circuit of QAE algorithm including single application of operator L in a 2-qubit case with an ancilla. (a) Operator L when Hadamard gates are involved in loading a distribution function. (b) Operator L when R_y rotations are used in loading a distribution function.

In this paper, up-state and down-state are considered as the system states for each component. Then, time duration of each state should be calculated. Analytically, if an exponential failure model is assumed, the time duration of a component which stays in up-state is time to failure (TTF) as given in (19a). Similarly, the time to repair (TTR) is used to describe the time duration of a component in down-state as (19b) [9, P.406], [24]:

$$TTF_m = -\frac{1}{\lambda_m} \cdot ln(U_1),\ m \in M \tag{19a}$$

$$TTR_m = -\frac{1}{\mu_m} \cdot ln(U_2),\ m \in M. \tag{19b}$$

where, λ_m and μ_m are failure rate and repair rate of the component m in the component set M, respectively. Also, the random numbers U_1 and U_2 are between 0 and 1. Numerically, those indices can be evaluated through Monte Carlo simulations, including probabilistic distributions and expected values.

In a distribution system, the faults occurring at lateral branches and main feeders are isolated by fuses and disconnects, respectively. To asses the distribution system reliability facing the faults, load-point and system-level indices are exploited. The load-point indices are calculated for each load using the random variables TTF and TTR of each component such as lines and cables. The load-point indices are defined as follows [56]:

$$\lambda_k = \frac{F_k}{\sum_t t_{up,k}},\ \forall k \in K, \tag{20a}$$

$$r_k = \frac{\sum_t t_{dn,k}}{F_k},\ \forall k \in K, \tag{20b}$$

$$U_k = \frac{\sum_t t_{dn,k}}{\sum_t t_{up,k} + \sum_t t_{dn,k}},\ \forall k \in K. \tag{20c}$$

where, λ_k, r_k and U_k are the average failure rate, the average outage time and average annual outage time of load point k, respectively. Also, $\sum_t t_{up,k}$ and $\sum_t t_{dn,k}$ are the total up and down times of load point k, respectively. F_k denotes the number of failures of load point k during the total sampled years.

The load-point metrics introduced in (20a)-(20c) are insufficient to elaborate the system behavior. To quantify the overall distribution system reliability, the system-level metrics such as customer-orientated and energy-orientated indices are introduced on top of the calculated load-point metrics. A detailed procedure of the classical MCS method to obtain the load point and system point indices are explained in [9]. In addition to indices for characterising momentary outages, the more widely used system reliability indices include system average interruption frequency index (SAIFI), system average interruption duration index (SAIDI), customer average interruption duration index (CAIDI), average service availability (unavailability) index (ASAI), energy not supplied index (ENS) and average energy not supplied index(AENS), which are formulated as follows [9, P.223], [57]:

$$SAIFI = \frac{\sum_k \lambda_k \cdot N_k}{\sum_k N_k}, \tag{21a}$$

$$SAIDI = \frac{\sum_k U_k \cdot N_k}{\sum_k N_k}, \tag{21b}$$

$$CAIDI = \frac{\sum_k U_k \cdot N_k}{\sum_k N_k \cdot \lambda_k}, \tag{21c}$$

$$ASAI = \frac{\sum_k N_k \times 8760 - \sum_k N_k U_k}{\sum_k N_k \times 8760}, \tag{21d}$$

$$ASUI = 1 - ASAI, \tag{21e}$$

$$ENS = \sum_k D_k \cdot U_k, \tag{21f}$$

$$AENS = \frac{\sum_k D_k \cdot U_k}{\sum_k N_k}. \tag{21g}$$

where, N_k and D_k are the number of customers and the average load demand at load point k, respectively.

B. Quantum-amenable reliability evaluation

This subsection aims at transforming a classical system reliability calculation into a quantumized reliability analytic.

This article has been accepted for publication in IEEE Transactions on Power Systems. This is the author's version which has not been fully edited and content may change prior to final publication. Citation information: DOI 10.1109/TPWRS.2022.3204393

To assess the load-point and system-level reliability indices using QAE, the following steps should be implemented:

Step1: Loading the probability distribution function of random variables U_1 and U_2. To obtain the TTF (19a) and TTR (19b), the random numbers U_1 and U_2 should be loaded using the quantum block $\mathcal{P}$. According to subsection. III-B, the random variable x in (2) is replaced by U_1 and U_2, and the probability of each variable is described by $p(U_1)$ and $p(U_2)$, respectively. To use the QAE algorithm to estimate quantities related to a random number U_1 or U_2, we should first represent U_1 or U_2 as a quantum state. A total of n qubits are utilized to map U_1 or U_2 to the interval $\{0, 1, \cdots, 2^n - 1\}$. After applying the quantum block $\mathcal{P}$ into an n-qubit register $|0\rangle_n$, the following quantum state output ($|\psi_{U_1}\rangle_n$ or $|\psi_{U_2}\rangle_n$) is resulted for each random variable with the corresponding probability:

$$|0\rangle_n \xrightarrow{\mathcal{P}} |\psi_{U_1}\rangle_n = \sum_{i_1=0}^{2^n-1} \sqrt{p_{i_1}} \cdot |i_1\rangle_n , \tag{22a}$$

$$|0\rangle_n \xrightarrow{\mathcal{P}} |\psi_{U_2}\rangle_n = \sum_{i_2=0}^{2^n-1} \sqrt{p_{i_2}} \cdot |i_2\rangle_n , \tag{22b}$$

where, $i_1, i_2 \in \{0, 1, \cdots, 2^n - 1\}$ are one of the 2^n possible realizations of U_1 and U_2, respectively. Moreover, $p_{i1} \in [0, 1]$ and $p_{i2} \in [0, 1]$ are the probability of measuring states $|i_1\rangle_n$ and $|i_2\rangle_n$, respectively. The measuring states associated with random variables U_1 and U_2 are represented by $|i_1\rangle_n$ and $|i_2\rangle_n$, respectively.

Step2: Calculating the TTF and TTR. In the QAE algorithm, to calculate the TTF, a quantum operator $\mathcal{H}_1$ is integrated into the quantum circuit such that $|w_1 \cdot ln(i_1)\rangle$ is calculated and the result is stored into the ancilla qubit with the state $|0\rangle$. In other words, the following state yields TTF state after applying $\mathcal{H}_1$ quantum block:

$$|\psi_{TTF}\rangle_n = |i_1\rangle_n |w_1 \cdot ln(i_1)\rangle , \tag{23}$$

where, $w_1 = -\frac{1}{\lambda_m}$.
Similarly, the quantum block $\mathcal{H}_2$ is employed to estimate TTR state using obtained state of U_2 and calculated $|w_2 \cdot ln(i_2)\rangle$. The resulted state of TTR is as follows:

$$|\psi_{TTR}\rangle_n = |i_2\rangle_n |w_2 \cdot ln(i_2)\rangle , \tag{24}$$

where, $w_2 = -\frac{1}{\mu_m}$.

Step3: Calculating the load-point reliability indices. In the third step, the average failure rate (λ_k), average outage time (r_k) and average annual outage time (U_k) of k^{th} load are calculated. To construct the quantum circuits associated with (20a)-(20c), we need the states of TTF($|\psi_{TTF}\rangle_n$) and TTR($|\psi_{TTR}\rangle_n$). From (20a)-(20c), quantum sum operators should be constructed after loading the quantum states of TTF and TTR. To estimate the λ_k, a quantum operator $\mathcal{H}_3$ should be used to yield the following state:

$$|\psi_{\lambda_k}\rangle_n = |\psi_{TTF}\rangle_n \left| \frac{w_3}{\sum_{i=1}^n TTF_i} \right\rangle , \tag{25}$$

where, w_3 is number of times the component fails (F_k in (20a)). Also, $|TTF\rangle_n = |TTF_1 TTF_2 \cdots TTF_n\rangle$. The result is stored in the ancilla qubit. Similarly, to estimate the r_k, a quantum operator $\mathcal{H}_4$ should be used to yield the following state:

$$|\psi_{r_k}\rangle_n = |\psi_{TTR}\rangle_n \left| \frac{\sum_{i=1}^n TTR_i}{w_3} \right\rangle , \tag{26}$$

where, $|TTR\rangle_n = |TTR_1 TTR_2 \cdots TTR_n\rangle$. Additionally, the quantum operator $\mathcal{H}_5$ is used to derive the quantum state of average annual outage time of load point k (U_k):

$$|\psi_{U_k}\rangle_n = |\psi_{TTF}\rangle_n |\psi_{TTR}\rangle_n \left| \frac{\sum_{i=1}^n TTR_i}{\sum_{i=1}^n TTF_i + \sum_{i=1}^n TTR_i} \right\rangle , \tag{27}$$

Step4: Calculating the system-point reliability indices. From step 1 to step 3, the required quantum blocks to estimate each system-level reliability index are constructed. The quantum block $\mathcal{P}$ is employed to construct the quantum state for random variables. Additionally, the quantum block $\mathcal{H}$ discussed in Section III is constructed as $\mathcal{H} = \mathcal{H}_1 \otimes \mathcal{H}_2 \otimes \mathcal{H}_3 \otimes \mathcal{H}_4 \otimes \mathcal{H}_5$. The quantum circuit to estimate each system-level reliability index is the combination of operators $\mathcal{P}$ and $\mathcal{H}$ ($\mathcal{H}(\mathcal{P} \otimes I) \cdot |0\rangle_n |0\rangle$), which ends up in the quantum block g. In the following, we extend the operator g to calculate the reliability index SAIFI:

$$|\psi_{SAIFI}\rangle_n = \sum_{i=0}^{2^n-1} \left[\sqrt{p(\lambda_i)} \cdot |\lambda_i\rangle_n \left(\sqrt{\frac{\sum_k \lambda_{k,i} \cdot N_k}{\sum_k N_k}} \cdot |1\rangle + \sqrt{1 - \frac{\sum_k \lambda_{k,i} \cdot N_k}{\sum_k N_k}} \cdot |0\rangle \right) \right] , \tag{28}$$

where, as it is theoretically discussed in Section III, the probability of measuring state $|1\rangle$ results in the SAIFI index estimation. Similarly, the quantum state associated with SAIDI is as follows:

$$|\psi_{SAIDI}\rangle_n = \sum_{i=0}^{2^n-1} \left[\sqrt{p(U_i)} \cdot |U_i\rangle_n \left(\sqrt{\frac{\sum_k U_{k,i} \cdot N_k}{\sum_k N_k}} \cdot |1\rangle + \sqrt{1 - \frac{\sum_k U_{k,i} \cdot N_k}{\sum_k N_k}} \cdot |0\rangle \right) \right] . \tag{29}$$

Step5: Efficient estimation of reliability metrics. To have an efficient estimation of each reliability index, S number application of quantum block L is used which is controlled by qubits in superposition state. The number of applications of block L in the QAE algorithm is equivalent to the sampling size in classical MCS method. Therefore, the quantum computing requires exponentially less samples compared to the classical MCS method. After performing an inverse Quantum Fourier Transform, the ancilla qubits are measured.

In classical MCS method and our quantum-based method (QAE), to estimate the accurate results, we increase the sampling size to assess the reliability indices. Furthermore, in the MCS method and QAE, random numbers ($U_1 \in [0, 1]$ and $U_2 \in [0, 1]$) are generated to calculate TTF and TTR of components; and to decrease the convergence errors, the number of samples are increased – this feature is not available in analytical methods. The quantum block L uses qubits to generate a large sampling size that current classical MCS methods might encounter scalability and computational issues. To decrease the convergence errors and mitigate the impact of outliers or some

unrealistic data, the QAE method uses many application of operator L to generate different scenarios, whereas in MCS methods, this strategy can be computationally expensive; even in analytical or machine learning-based techniques, wrong input distribution functions results in wrong outputs.

A flowchart is depicted as Fig. 8 to describe the Quantum-amenable reliability assessment process.

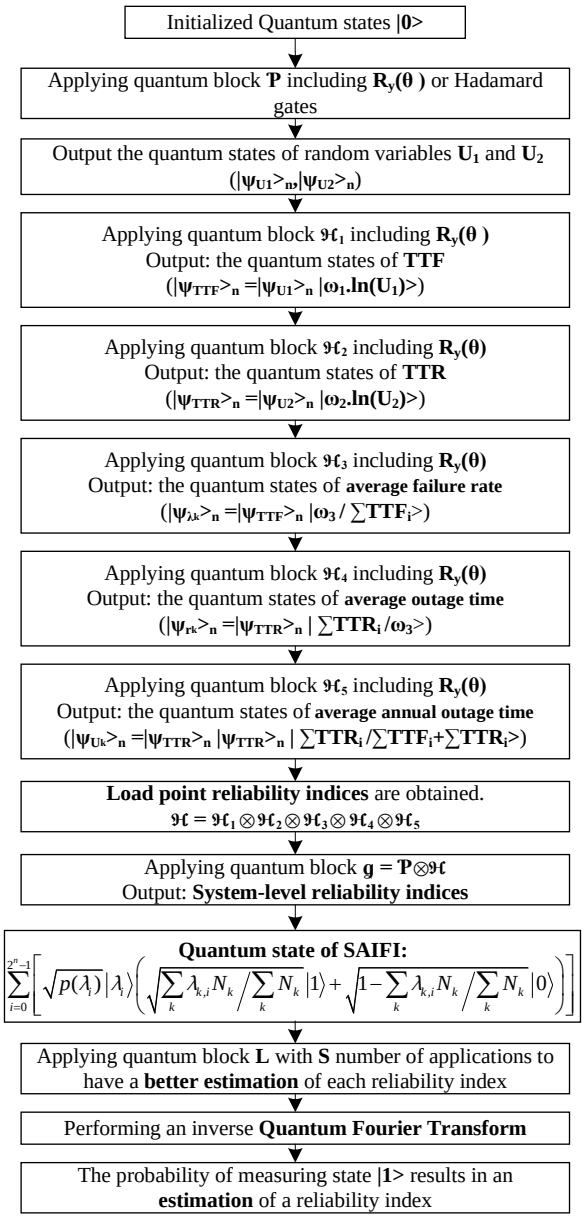

Fig. 8. A flowchart of quantum computing for reliability indices evaluation

In the mathematical formulations to obtain the reliability indices, we employ the summation operator. For example, three component gates are required to construct the summation operator for reliability indices. The required steps to build the summation operator required to calculate load-point and system-point indices are shown in Fig. 9.

To calculate the reliability indices, the summation operator is needed. Therefore, to convert the classical mathematical equations into summation operators, we need the following steps to run using quantum gates:

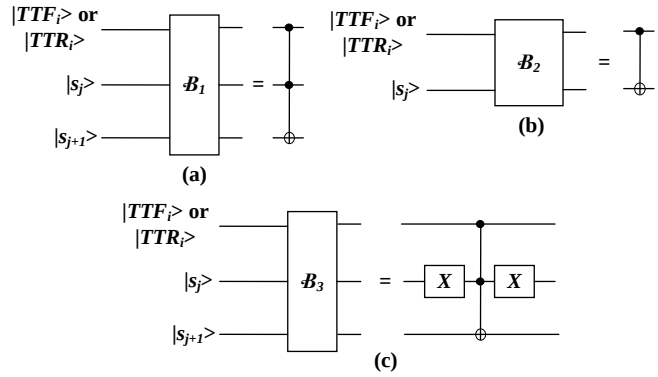

Fig. 9. Steps to construct summation operator in the quantum circuit used for reliability indices assessment.

- A quantum operator $\mathcal{B}_1$, which is equivalent to a Toffoli gate, is used to compute the carry from adding state $|TTF_i\rangle$ or $|TTR_i\rangle$ and state $|s_j\rangle$ into state $|s_{j+1}\rangle$. In other words, operator $\mathcal{B}_1$ is a summation operator to compute the arithmetic sum of the values of n qubits $|TTF\rangle_n = |TTF_1\ TTF_2 \cdots\ TTF_n\rangle$ or $|TTR\rangle_n = |TTR_1\ TTR_2 \cdots\ TTR_n\rangle$, and the summation results are stored in m-qubit register $|s\rangle_m = |s_1\ s_2 \cdots s_m\rangle$.
- The quantum operator $\mathcal{B}_2$, which consists of a CNOT gate, adds the the state qubit $|TTF_i\rangle$ or $|TTR_i\rangle$ to the qubit $|s_j\rangle$. This operator is shown in Fig. 9(b).
- The operator $\mathcal{B}_3$, which consists of a Toffoli gate and two NOT (X) gates, resets the carry qubit (ancilla qubit) back to $|0\rangle$.

V. Numerical results

In this section, to validate our quantum reliability model, a 4-bus case study is first considered. Then, the practicality and efficacy of the quantum-amenable model are tested on the 33-bus and 119-bus radial and mesh distribution systems, where the number of components are increased. To design the quantum circuit and run the quantum algorithm, the IBM statevector simulator is employed.

A. Four-bus radial distribution system

In this case study, a 4-bus radial distribution system used in [9, p.230] is considered to assess the reliability indices. As depicted in Fig. 10, the system comprises 4 load nodes, 4 lateral branches and 4 distribution lines. Three different scenarios are analyzed. In the first scenario, which is a base case, the reliability indices are assessed without considering protection systems and isolators. In the second scenario, only fuses are exploited in lateral branches. In the last scenario, in addition to fuses, isolators or disconnects are considered as part of the distribution lines.

1) Four-bus radial distribution grid without protection systems: In this scenario, none of the protection devices on the distribution feeders (Ω_1, Ω_2, Ω_3, and Ω_4) and laterals (Γ_1, Γ_2, Γ_3, and Γ_4) are included. Therefore, any failures along each line or cable will cause the main breaker to be opened and none of the load points ($\mathcal{D}_1$, $\mathcal{D}_2$, $\mathcal{D}_3$, and $\mathcal{D}_4$) will be supplied. The reliability parameters of the radial distribution system are taken

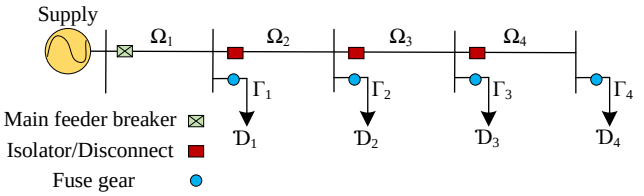

Fig. 10. Single line diagram of 4-bus radial distribution system including protection systems.

from [9, Table 7.7, p.230]. Additionally, the data associated with load points are available in [9, Table 7.9, p.232].

Table I summarizes the system reliability indices (expected values) obtained from quantum and classical methods.

TABLE I
SYSTEM-LEVEL RELIABILITY INDICES ASSESSMENT IN 4-BUS RADIAL DISTRIBUTION SYSTEM WITHOUT PROTECTION SYSTEM (FIRST SCENARIO)

Method	System point indices		
	SAIFI (interruptions/year)	SAIDI (hours/year)	CAIDI (hours/interruption)
QAE	2.191	6.04	2.71
SMCS [9]	2.195	5.92	2.69
Analytical [9]	2.2	6	2.73
Method	ASAI	ENS (MWh/year)	AENS (kWh/customer.year)
QAE	0.9993	84.13	27.89
SMCS [9]	0.9993	84.8	27.64
Analytical [9]	0.9993	84	28

From Table I, to check the accuracy of the QAE algorithm compared to the analytical method, the error of SAIFI, SAIDI, CAIDI, ENS, and AENS are 0.41%, 0.67%, 0.73%, 0.15%, and 0.39%, respectively.

2) Four-bus radial distribution grid entailing fuses in lateral branches: In this scenario, the fuse gear is installed on each lateral while the line isolators/disconnects in Fig. 10 are disregarded. In case a failure occurs on a lateral feeder, the fuse operates and the lateral disconnects from its load point until the faulted feeder is repaired/restored while the other load points will be in the connected mode. All input data are the same as the first scenario.

TABLE II
SYSTEM-LEVEL RELIABILITY INDICES ASSESSMENT IN 4-BUS RADIAL DISTRIBUTION SYSTEM IN PRESENCE OF THE FUSE GEAR IN EACH LATERAL BRANCH (SECOND SCENARIO)

Method	System point indices		
	SAIFI (interruptions/year)	SAIDI (hours/year)	CAIDI (hours/interruption)
QAE	1.146	3.93	3.37
SMCS	1.16	3.94	3.38
Analytical [9]	1.15	3.91	3.37
Method	ASAI	ENS (MWh/year)	AENS (kWh/customer.year)
QAE	0.9995	54.4	18.2
SMCS	0.9995	55.3	18.4
Analytical [9]	0.9995	54.8	18.3

In Table II, the expected system reliability indices are evaluated using QAE in the 4-bus radial distribution system and compared with those obtained by classical sequential MCS and analytical techniques in [9, p.232].

According to the results described in Table II, the percentage errors of quantum computing compared to the analytical method are 0.35%, 0.5%, 0.15%, 0.73%, and 0.5% for SAIFI, SAIDI, CAIDI, ENS, and AENS, respectively.

3) Four-bus radial distribution system including lateral feeder protection and isolators/disconnects: To evaluate the reliability indices, in addition to lateral fuses, isolators/disconnects are installed on the feeder sections. Under this type of protection scheme, any failure on a feeder causes the main breaker to operate until the the fault is detected. Upon the fault detection, the isolator operates and all load points between the supply and the isolator are restored. In this scenario, the isolation time should be considered [9, p.234]. To analyze the effect of isolators/disconnects on the reliability indices of the distribution system of Fig. 10, the results from the QAE algorithm is represented in Table III.

TABLE III
SYSTEM-LEVEL RELIABILITY INDICES ASSESSMENT IN 4-BUS RADIAL DISTRIBUTION SYSTEM IN PRESENCE OF FUSE GEARS ON LATERAL BRANCHES AND ISOLATORS ON DISTRIBUTION LINES (THIRD SCENARIO)

Method	System point indices		
	SAIFI (interruptions/year)	SAIDI (hours/year)	CAIDI (hours/interruption)
QAE	1.157	2.57	2.24
SMCS [9]	1.158	2.55	2.20
Analytical	1.159	2.59	2.23
Method	ASAI	ENS (MWh/year)	AENS (kWh/customer.year)
QAE	0.9997	35.2	11.69
SMCS [9]	0.9997	35.2	11.7
Analytical	0.9997	35.3	11.79

After comparing the obtained results from Table III, the error of reliability indices SAIFI, SAIDI, CAIDI, ENS, and AENS using QAE are 0.17%, 0.7%, 0.45%, 0.28%, and 0.85%, respectively.

B. 33-bus radial distribution system

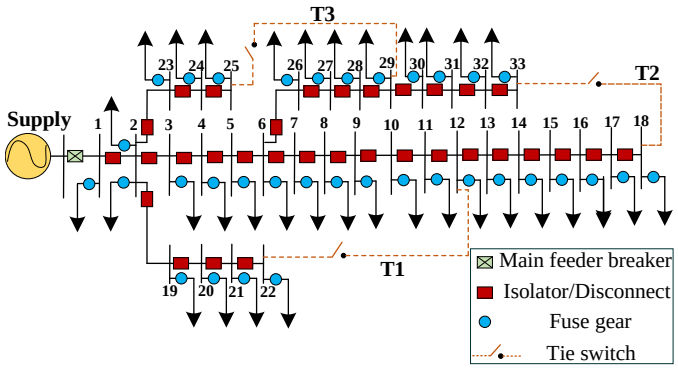

Fig. 11. Single line diagram of 33-bus distribution system including protection systems.

To validate the scalability of quantum computing in distribution system reliability assessment, the size of the distribution grid is increased such that more components such as load points, distribution lines, isolators, and lateral branches are considered. In Fig. 11, the single line diagram of the 33-bus distribution system containing protection systems is depicted.

In this case study, the tie-lines are ignored. In Table IV, Table V and Table VI, the results of system-level reliability evaluation are represented in three scenarios.

TABLE IV
SYSTEM-LEVEL RELIABILITY INDICES ASSESSMENT FOR 33-BUS RADIAL DISTRIBUTION SYSTEM WITHOUT PROTECTION SYSTEMS (FIRST SCENARIO)

Indices	Method			Error (%)
	QAE	SMCS	Analytical	
SAIFI (interruptions/year)	18.21	18.30	18.18	0.17
SAIDI (hours/year)	49.63	50.03	49.69	0.12
CAIDI (hours/interruption)	2.72	2.73	2.73	0.37
Indices	QAE	SMCS	Analytical	Error (%)
ASAI	0.9945	0.9942	0.9943	0.002
ENS (MWh/year)	5816.3	5853.7	5814.3	0.003
AENS (kWh/customer.year)	232.30	234.15	232.57	0.12

TABLE V
SYSTEM-LEVEL RELIABILITY INDICES ASSESSMENT FOR 33-BUS RADIAL DISTRIBUTION SYSTEM IN PRESENCE OF THE FUSE GEAR IN EACH LATERAL BRANCH (SECOND SCENARIO)

Indices	Method			Error (%)
	QAE	SMCS	Analytical	
SAIFI (interruptions/year)	6.98	7.06	7.02	0.57
SAIDI (hours/year)	27.39	27.55	27.37	0.01
CAIDI (hours/interruption)	3.86	3.9	3.9	1.0
Indices	QAE	SMCS	Analytical	Error (%)
ASAI	0.9968	0.9968	0.9969	0.001
ENS (MWh/year)	3181.94	3224.5	3202.9	0.65
AENS (kWh/customer.year)	127.68	128.98	128.11	0.34

TABLE VI
SYSTEM-LEVEL RELIABILITY INDICES ASSESSMENT FOR 33-BUS RADIAL DISTRIBUTION SYSTEM IN PRESENCE OF FUSE GEARS IN LATERAL BRANCHES AND ISOLATORS IN DISTRIBUTION LINES (THIRD SCENARIO)

Indices	Method			Error (%)
	QAE	SMCS	Analytical	
SAIFI (interruptions/year)	7.01	7.06	6.98	0.4
SAIDI (hours/year)	9.96	10.03	9.94	0.2
CAIDI (hours/interruption)	1.43	1.42	1.423	0.5
Indices	QAE	SMCS	Analytical	Error (%)
ASAI	0.9989	0.9988	0.9989	0.001
ENS (MWh/year)	1155.75	1178.38	1164.82	0.7
AENS (kWh/customer.year)	46.90	47.13	46.59	0.6

From obtained results by QAE (Table IV, Table V and Table VI), it is seen that, in all scenarios for each reliability index, the percentage errors of the quantum reliability results are between 0 and 1% as compared to those from the analytical method.

C. 33-bus mesh distribution system

In this case study, we consider all the tie-lines in Fig. 11. Tie-lines T1, T2 and T3 are employed to connect buses 12 and 22, buses 18 and 33, and buses 25 and 29, respectively. The system reliability indices in presence of fuses and isolators in line sections are assessed using three methods, as summarized in Table VII.

TABLE VII
SYSTEM-LEVEL RELIABILITY INDICES ASSESSMENT IN 33-BUS MESH DISTRIBUTION SYSTEM IN PRESENCE OF FUSE GEARS IN LATERAL BRANCHES AND ISOLATORS IN DISTRIBUTION LINES

Indices	Method			Error (%)
	QAE	SMCS	Analytical	
SAIFI (interruptions/year)	6.96	7.10	7.02	0.8
SAIDI (hours/year)	6.38	6.44	6.34	0.6
CAIDI (hours/interruption)	0.901	0.903	0.904	0.3
Indices	QAE	MCS	Analytical	Error (%)
ASAI	0.9993	0.9993	0.9993	0.01
ENS (MWh/year)	738.40	752.96	741.62	0.4
AENS (kWh/customer.year)	29.44	30.11	29.66	0.7

D. 119-bus distribution system

In this case study, a large 119-bus distribution system with two scenarios, radial structure and mesh structure is considered. In addition, fuse gears in branches and isolators in distribution lines are included in both scenarios. In Fig. 12, the schematic diagram of the 119-bus distribution system is depicted [58].

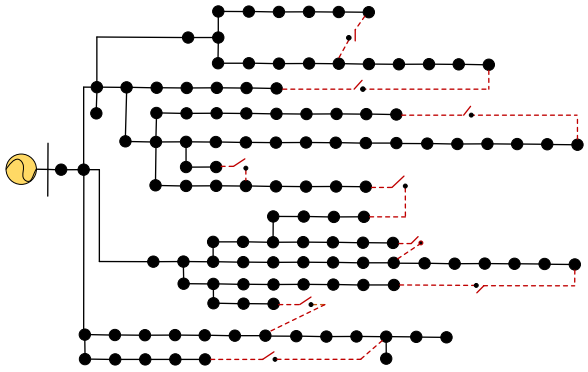

Fig. 12. Single line diagram of 119-bus distribution system.

1) 119-bus radial distribution system: In the first scenario, a radial distribution system with no connection between the sub-feeders is considered, and therefore, the tie-line switches are open. In Table VIII, the reliability indices of the 119-bus radial distribution system obtained by QAE, classical SMCS and the analytical approach are compared.

Compared to the analytical method, the percentage errors of the QAE algorithm is low, which shows the accuracy of the quantum-inspired method.

In Fig. 13, the probability distribution function of two reliability indices are depicted in 119-bus radial distribution system.

This article has been accepted for publication in IEEE Transactions on Power Systems. This is the author's version which has not been fully edited and content may change prior to final publication. Citation information: DOI 10.1109/TPWRS.2022.3204393

TABLE VIII
SYSTEM-LEVEL RELIABILITY INDICES ASSESSMENT FOR 119-BUS RADIAL DISTRIBUTION SYSTEM IN PRESENCE OF FUSE GEARS IN LATERAL BRANCHES AND ISOLATORS IN DISTRIBUTION LINES

Indices	Method			Error (%)
	QAE	SMCS	Analytical	
SAIFI (interruptions/year)	24.68	25.42	24.56	0.49
SAIDI (hours/year)	19.56	20.01	19.33	1.1
CAIDI (hours/interruption)	0.78	0.78	0.78	0.1
Indices	QAE	SMCS	Analytical	Error (%)
ASAI	0.9978	0.9977	0.9978	0.01
ENS (MWh/year)	8169.27	8202.15	8082.66	1.0
AENS (kWh/customer.year)	90.98	91.57	90.31	0.74

TABLE IX
SYSTEM RELIABILITY INDICES ASSESSMENT FOR 119-BUS MESHED DISTRIBUTION SYSTEM IN PRESENCE OF FUSE GEARS IN LATERAL BRANCHES AND ISOLATORS IN DISTRIBUTION LINES

Indices	Method			Error (%)
	QAE	SMCS	Analytical	
SAIFI (interruptions/year)	24.47	24.99	24.39	0.32
SAIDI (hours/year)	15.36	15.55	15.18	1.2
CAIDI (hours/interruption)	0.62	0.62	0.62	0.01
Indices	QAE	SMCS	Analytical	Error (%)
ASAI	0.9982	0.9982	0.9983	0.01
ENS (MWh/year)	6399.34	6498.63	6345.27	0.8
AENS (kWh/customer.year)	71.52	71.96	70.90	0.87

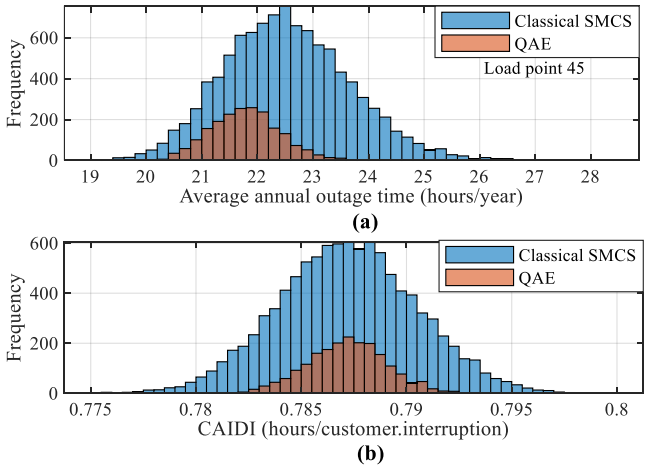

Fig. 13. Probability distributions of reliability indices: (a) annual outage duration of bus 45. (b) CAIDI.

In Fig. 13(a) and Fig. 13(b), the probability distribution functions of the average annual outage time index (load-point index) and customer average interruption duration index (system-level index) are shown, respectively. The distribution functions obtained by QAE is compared to those by the classical SMCS method. It is seen that the QAE algorithm guarantees the convergence with small sampling size compared to the classical SMCS method.

2) 119-bus mesh distribution system: In this scenario, nine tie-lines are considered, where the associated switches operate in the closed mode. Table IX compares the performance of different methods in calculating the reliability indices.

The results of Table IX indicate lower percentage errors of the QAE over the classical SMCS method.

Discussion: Current quantum machines have experienced a rapid progress from scalability and performance points of view, and are now approaching to a promising computing point to solve those engineering problems that cannot be tackled by the classical counterparts. This could make a revolution for solving industrial problems. Current limitations of classical methods motivated us to develop a new method based on quantum computing. According to the results obtained in different case studies, the quantum computing demonstrated a guaranteed methodology to assess the reliability indices. As theoretically discussed, the quadratic speed-up of convergence is achievable using quantum-amenable MCS method compared to the classical counterpart. Moreover, to load the distribution function of random variables, the QAE algorithm employs qubits for sampling, that is an efficient alternative for the required sampling size in the classical MCS method to achieve the reliable answers. Therefore, the classical sequential MCS is a computationally expensive method due to its dependency on large number of samples, whereas the quantum-inspired method uses a small number of qubits to produce the quantum samples sufficient for the accurate estimation of reliability indices. As a comparison, Fig. 14 depicts the convergence of classical MCS with increased sampling sizes in obtaining SAIFI of the 33-bus mesh distribution system including all protection systems.

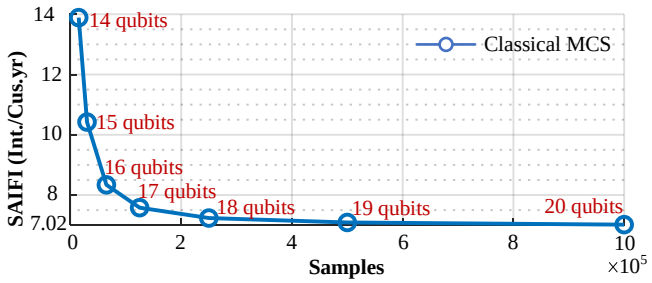

Fig. 14. Convergence of SAIFI index in 33-bus mesh distribution system in different sampling size. The required number of qubits to produce the same sampling size is also shown.

In Fig. 14, the required number of qubits for the classical sampling using the MCS method is represented. To load a distribution function containing 10^6 samples in the classical framework, 20 qubits is sufficient. Even with today's Noisy Intermediate-Scale Quantum (NISQ) devices with limited qubits, the power system reliability assessment is readily executable using our quantum algorithm. For instance, the QAE algorithm required 14 qubits to load the required samples to assess the reliability indices of 33-bus mesh distribution system.

To compare the computational time of the quantum-inspired algorithm over the classical SMCS method, Table X is provided.

From Table X, the QAE algorithm obtains the reliability indices more efficiently as compared to the classical SMCS

TABLE X
COMPUTATIONAL SPEEDS FOR DIFFERENT METHODS TESTED ON RADIAL AND MESH DISTRIBUTION SYSTEMS

Structure (Method)	System size		
	4-bus	33-bus	119-bus
Radial (QAE)	8 (s)	55 (s)	241 (s)
Radial (SMCS)	39 (s)	382 (s)	1471 (s)
Mesh (QAE)	9 (s)	62 (s)	265 (s)
Mesh (SMCS)	44 (s)	401 (s)	1512 (s)

method.

VI. CONCLUSION

In this paper, for the first time, the quantum computing was introduced and used to evaluate the reliability indices in distribution systems. The quantum-amenable model of the distribution system reliability was developed and the quantum amplitude estimation algorithm was employed to execute the quantum circuit containing the probability distribution loading block for random variables, estimation of required functions of random variables, and measuring units. According to the results, the quantum MCS could achieve the same reliability indices as the classical MCS method and analytical technique. Compared to the classical MCS method in which the sampling size determines the convergence rate of the method, the quantum MCS needed a small number of qubits to produce the same results with quadratic speed-up of convergence. This achievement by quantum computing is a promising step towards evaluating the reliability indices for large-scale systems where the classical MCS would be unable to tackle it. As a future plan, a quantum-amenable reliability-constrained optimization model is to be investigated for microgrids.

ACKNOWLEDGEMENT

We would like to thank the Brookhaven National Laboratory operated IBM-Q Hub. This research used resources of the Oak Ridge Leadership Computing Facility, which is a DOE Office of Science User Facility supported under Contract DE-AC05-00OR22725.

REFERENCES

[1] R. Billinton and R. N. Allan, "Power-system reliability in perspective," *Electronics and Power*, vol. 30, no. 3, pp. 231–236, 1984.

[2] W.-C. Yeh, "An improved sum-of-disjoint-products technique for symbolic multi-state flow network reliability," *IEEE Transactions on Reliability*, vol. 64, no. 4, pp. 1185–1193, 2015.

[3] M. Jooshaki, A. Abbaspour, M. Fotuhi-Firuzabad, G. Munoz-Delgado, J. Contreras, M. Lehtonen, and J. M. Arroyo, "An enhanced milp model for reliability-constrained distribution network expansion planning," *IEEE Transactions on Power Systems*, 2021.

[4] R. He, H. Xie, J. Deng, T. Feng, L. L. Lai, and M. Shahidehpour, "Reliability modeling and assessment of cyber space in cyber-physical power systems," *IEEE Transactions on Smart Grid*, vol. 11, no. 5, pp. 3763–3773, 2020.

[5] A. Tabares, G. Munoz-Delgado, J. F. Franco, J. M. Arroyo, and J. Contreras, "An enhanced algebraic approach for the analytical reliability assessment of distribution systems," *IEEE Transactions on Power Systems*, vol. 34, no. 4, pp. 2870–2879, 2019.

[6] P. Zhang and W. Li, "Boundary analysis of distribution reliability and economic assessment," *IEEE Transactions on Power Systems*, vol. 25, no. 2, pp. 714–721, 2010.

[7] A. A. Eajal, A. El-Awady, E. F. El-Saadany, K. Ponnambalam, A. Al-Durra, A. S. Al-Sumaiti, and M. M. Salama, "A bayesian approach to the reliability analysis of renewables-dominated islanded dc microgrids," *IEEE Transactions on Power Systems*, vol. 36, no. 5, pp. 4296–4309, 2021.

[8] K. Hou, H. Jia, X. Xu, Z. Liu, and Y. Jiang, "A continuous time markov chain based sequential analytical approach for composite power system reliability assessment," *IEEE Transactions on Power Systems*, vol. 31, no. 1, pp. 738–748, 2015.

[9] R. N. Allan *et al.*, *Reliability evaluation of power systems*. Springer Science & Business Media, 2013.

[10] G. Li, P. Zhang, P. B. Luh, W. Li, Z. Bie, C. Serna, and Z. Zhao, "Risk analysis for distribution systems in the northeast u.s. under wind storms," *IEEE Transactions on Power Systems*, vol. 29, no. 2, pp. 889–898, 2014.

[11] R. Billinton and G. Bai, "Generating capacity adequacy associated with wind energy," *IEEE transactions on energy conversion*, vol. 19, no. 3, pp. 641–646, 2004.

[12] R. Billinton, H. Chen, and R. Ghajar, "Time-series models for reliability evaluation of power systems including wind energy," *Microelectronics Reliability*, vol. 36, no. 9, pp. 1253–1261, 1996.

[13] E. Tomasson and L. Söder, "Generation adequacy analysis of multi-area power systems with a high share of wind power," *IEEE Transactions on Power Systems*, vol. 33, no. 4, pp. 3854–3862, 2017.

[14] Z. Bie, P. Zhang, G. Li, B. Hua, M. Meehan, and X. Wang, "Reliability evaluation of active distribution systems including microgrids," *IEEE Transactions on Power Systems*, vol. 27, no. 4, pp. 2342–2350, 2012.

[15] J. Zhu and Y. Zhang, "A frequency and duration method for adequacy assessment of generation systems with wind farms," *IEEE Transactions on Power Systems*, vol. 34, no. 2, pp. 1151–1160, 2018.

[16] A. L. Da Silva, L. D. F. Manso, J. D. O. Mello, and R. Billinton, "Pseudo-chronological simulation for composite reliability analysis with time varying loads," *IEEE Transactions on Power Systems*, vol. 15, no. 1, pp. 73–80, 2000.

[17] R. A. Gonzalez-Fernandez and A. M. L. da Silva, "Reliability assessment of time-dependent systems via sequential cross-entropy monte carlo simulation," *IEEE Transactions on Power Systems*, vol. 26, no. 4, pp. 2381–2389, 2011.

[18] Z. Li, W. Wu, X. Tai, and B. Zhang, "A reliability-constrained expansion planning model for mesh distribution networks," *IEEE Transactions on Power Systems*, vol. 36, no. 2, pp. 948–960, 2020.

[19] G. Muñoz-Delgado, J. Contreras, and J. M. Arroyo, "Reliability assessment for distribution optimization models: A non-simulation-based linear programming approach," *IEEE Transactions on Smart Grid*, vol. 9, no. 4, pp. 3048–3059, 2016.

[20] Z. Li, W. Wu, B. Zhang, and X. Tai, "Analytical reliability assessment method for complex distribution networks considering post-fault network reconfiguration," *IEEE Transactions on Power Systems*, vol. 35, no. 2, pp. 1457–1467, 2019.

[21] Z. Li, W. Wu, X. Tai, and B. Zhang, "Optimization model-based reliability assessment for distribution networks considering detailed placement of circuit breakers and switches," *IEEE Transactions on Power Systems*, vol. 35, no. 5, pp. 3991–4004, 2020.

[22] D. Urgun and C. Singh, "A hybrid monte carlo simulation and multi label classification method for composite system reliability evaluation," *IEEE Transactions on Power Systems*, vol. 34, no. 2, pp. 908–917, 2018.

[23] M. Kamruzzaman, N. Bhusal, and M. Benidris, "A convolutional neural network-based approach to composite power system reliability evaluation," *International Journal of Electrical Power & Energy Systems*, vol. 135, p. 107468, 2022.

[24] S. Li, T. Ding, C. Mu, C. Huang, and M. Shahidehpour, "A machine learning-based reliability evaluation model for integrated power-gas systems," *IEEE Transactions on Power Systems*, 2021.

[25] T. Lin and C. Shang, "Reliability evaluation on a joint machine learning and optimization framework," *IEEE Transactions on Power Systems*, vol. 36, no. 1, pp. 49–57, 2020.

[26] N. Nikmehr, P. Zhang, and M. Bragin, "Quantum distributed unit commitment: An application in microgrids," *IEEE transactions on power systems*, 2022.

[27] J. Preskill, "Quantum computing in the nisq era and beyond," *Quantum*, vol. 2, p. 79, 2018.

[28] A. Montanaro, "Quantum speedup of monte carlo methods," *Proceedings of the Royal Society A: Mathematical, Physical and Engineering Sciences*, vol. 471, no. 2181, p. 20150301, 2015.

[29] R. Y. Rubinstein and D. P. Kroese, *Simulation and the Monte Carlo method*. John Wiley & Sons, 2016, vol. 10.

[30] S. Heinrich, "Quantum summation with an application to integration," *Journal of Complexity*, vol. 18, no. 1, pp. 1–50, 2002.

[31] G. Brassard, P. Hoyer, M. Mosca, and A. Tapp, "Quantum amplitude amplification and estimation," *Contemporary Mathematics*, vol. 305, pp. 53–74, 2002.

[32] P. Wocjan, C.-F. Chiang, D. Nagaj, and A. Abeyesinghe, "Quantum algorithm for approximating partition functions," *Physical Review A*, vol. 80, no. 2, p. 022340, 2009.

[33] D. J. Tylavsky and G. T. Heydt, "Quantum computing in power system simulation," in *2003 IEEE Power Engineering Society General Meeting (IEEE Cat. No. 03CH37491)*, vol. 2. IEEE, 2003, pp. 950–956.

[34] F. Feng, Y. Zhou, and P. Zhang, "Quantum power flow," *IEEE Transactions on Power Systems*, vol. 36, no. 4, pp. 3810–3812, 2021.

[35] Y. Zhou, F. Feng, and P. Zhang, "Quantum electromagnetic transients program," *IEEE Transactions on Power Systems*, vol. 36, no. 4, pp. 3813–3816, 2021.

[36] Y. Zhou, P. Zhang, and F. Feng, "Noisy-intermediate-scale quantum electromagnetic transients program," *IEEE Transactions on Power Systems*, 2022.

[37] J. Sun, B. Feng, and W. Xu, "Particle swarm optimization with particles having quantum behavior," in *Proceedings of the 2004 congress on evolutionary computation (IEEE Cat. No. 04TH8753)*, vol. 1. IEEE, 2004, pp. 325–331.

[38] M. S. Alvarez-Alvarado and D. Jayaweera, "A new approach for reliability assessment of a static v ar compensator integrated smart grid," in *2018 IEEE International Conference on Probabilistic Methods Applied to Power Systems (PMAPS)*. IEEE, 2018, pp. 1–7.

[39] W. Xuan, Z. Zhao, L. Fan, and Z. Han, "Minimizing delay in network function visualization with quantum computing," in *2021 IEEE 18th International Conference on Mobile Ad Hoc and Smart Systems (MASS)*. IEEE, 2021, pp. 108–116.

[40] L. K. Grover, "Quantum mechanics helps in searching for a needle in a haystack," *Physical review letters*, vol. 79, no. 2, p. 325, 1997.

[41] S. Woerner and D. J. Egger, "Quantum risk analysis," *npj Quantum Information*, vol. 5, no. 1, pp. 1–8, 2019.

[42] C. Zoufal, A. Lucchi, and S. Woerner, "Quantum generative adversarial networks for learning and loading random distributions," *npj Quantum Information*, vol. 5, no. 1, pp. 1–9, 2019.

[43] Y. Suzuki, S. Uno, R. Raymond, T. Tanaka, T. Onodera, and N. Yamamoto, "Amplitude estimation without phase estimation," *Quantum Information Processing*, vol. 19, no. 2, pp. 1–17, 2020.

[44] M. A. Nielsen and I. L. Chuang, *Quantum Computation and Quantum Information: 10th Anniversary Edition*. Cambridge University Press, 2010.

[45] G. Chiribella, G. M. D'Ariano, and P. Perinotti, "Quantum circuit architecture," *Physical review letters*, vol. 101, no. 6, p. 060401, 2008.

[46] D. Bouwmeester and A. Zeilinger, "The physics of quantum information: basic concepts," in *The physics of quantum information*. Springer, 2000, pp. 1–14.

[47] A. Montanaro, "Quantum algorithms: an overview," *npj Quantum Information*, vol. 2, no. 1, pp. 1–8, 2016.

[48] R. Y. Rubinstein, *Simulation and the Monte Carlo Method*, ser. Wiley series in probability and mathematical statistics. Wiley, 1981.

[49] T. Tanaka, Y. Suzuki, S. Uno, R. Raymond, T. Onodera, and N. Yamamoto, "Amplitude estimation via maximum likelihood on noisy quantum computer," *Quantum Information Processing*, vol. 20, no. 9, pp. 1–29, 2021.

[50] P. Rebentrost, B. Gupt, and T. R. Bromley, "Quantum computational finance: Monte carlo pricing of financial derivatives," *Physical Review A*, vol. 98, no. 2, p. 022321, 2018.

[51] D. Grinko, J. Gacon, C. Zoufal, and S. Woerner, "Iterative quantum amplitude estimation," *npj Quantum Information*, vol. 7, no. 1, pp. 1–6, 2021.

[52] P. Glasserman, P. Heidelberger, and P. Shahabuddin, *Efficient Monte Carlo methods for value-at-risk*. IBM Thomas J. Watson Research Division, 2000.

[53] M. M. O. Onen, J. Vartiainen, V. Bergholm, and M. M. Salomaa, "Transformation of quantum states using uniformly controlled rotations," *Quantum Information and Computation*, vol. 5, no. 6, pp. 467–473, 2005.

[54] L. Grover and T. Rudolph, "Creating superpositions that correspond to efficiently integrable probability distributions," *arXiv preprint quant-ph/0208112*, 2002.

[55] M. Žnidarič, O. Giraud, and B. Georgeot, "Optimal number of controlled-not gates to generate a three-qubit state," *Physical Review A*, vol. 77, no. 3, p. 032320, 2008.

[56] R. Billinton and P. Wang, "Teaching distribution system reliability evaluation using monte carlo simulation," *IEEE Transactions on Power Systems*, vol. 14, no. 2, pp. 397–403, 1999.

[57] J. Dong, L. Zhu, Q. Dong, P. Kritprajun, Y. Liu, Y. Liu, L. M. Tolbert, J. Hambrick, Y. Xue, B. Ollis *et al.*, "Integrating transactive energy into reliability evaluation for a self-healing distribution system with microgrid," *IEEE Transactions on Sustainable Energy*, 2021.

[58] D. Zhang, Z. Fu, and L. Zhang, "An improved ts algorithm for loss-minimum reconfiguration in large-scale distribution systems," *Electric power systems research*, vol. 77, no. 5-6, pp. 685–694, 2007.

Nima Nikmehr (Senior Member, IEEE) is currently working toward the Ph.D. degree in electrical engineering with the department of Electrical and Computer Engineering, Stony Brook University, Stony Brook, NY, USA. He is an academic summer intern for Summer 2022 with Commonwealth Edison (ComEd). His research interests include power system operation and optimization, networked microgrids and quantum computing.

Nima Nikmehr received the Best Paper Award at the 2022 IEEE Power and Energy Society General Meeting for his research on quantum distributed unit commitment. He was also a recipient of the Outstanding Reviewer Award for IEEE Transactions on Sustainable Energy in 2021.

Peng Zhang (Senior Member, IEEE) received the Ph.D. degree in electrical engineering from the University of British Columbia, Vancouver, BC, Canada, in 2009. He is a Full Professor of Electrical and Computer Engineering, and a SUNY Empire Innovation Professor at Stony Brook University, New York. He has a joint appointment at Brookhaven National Laboratory as a Staff Scientist. Previously, he was a Centennial Associate Professor and a Francis L. Castleman Associate Professor at the University of Connecticut, Storrs, CT, USA. He was a System Planning Engineer at BC Hydro and Power Authority, Canada, during 2006-2010. His research interests include AI-enabled smart grids, quantum-engineered power grids, networked microgrids, power system stability and control, cybersecurity, and formal methods and reachability analysis.

Dr. Zhang is an individual member of CIGRÉ. He is an Editor for the IEEE Transactions on Power Systems, the IEEE Power and Energy Society Letters, and the IEEE Journal of Oceanic Engineering.